Temperature Assessment During Radio Frequency Ablation in Ex Vivo Long Bone by Fiber Bragg Grating Sensors

Francesca De Tommasi, *Student Member, IEEE*, Emiliano Schena, *Senior Member, IEEE*, Massimiliano Carassiti, Paul Jutte, Venkatasubramanian Kalpathy Venkiteswaran, *Member, IEEE*, and Sarthak Misra, *Senior Member, IEEE*

***Abstract*—Thermal ablation treatments (TATs) are promising alternatives to traditional surgery for bone cancer eradication. Among several TATs, radio frequency ablation (RFA) has gained considerable ground in treating bone cancer. Therefore, tracking temperature is paramount in ensuring complete tumor destruction without injuring adjacent structures. Despite the widespread use of RFA for bone tumors, investigations on temperature distribution during this procedure are so far lacking. To date, only thermocouples and thermistors have been proposed to measure temperature during RFA in bone. However, these sensors are intended to measure temperature at a single point without information about heat propagation into the tissue during ablation. Within this context, fiber Bragg grating sensors (FBGs) can play a crucial role since their multiplexing capability enables temperature measurement at several locations. This work seeks to fill this gap by providing new insights into RFA effects on bone tissue. Experiments are performed on ex vivo porcine femurs. During trials, two commercial stainless-steel needles equipped with an optical fiber housing six FBGs each were employed to record temperature over time. This solution allowed for monitoring temperature in 12 tissue points inside the bone at a fixed distance from the RF probe, thus gaining information about the thermal distribution in a large tissue area over time. This study paves the way for a more in-depth understanding of the efficacy of RFA in bone tissue, thus providing a powerful method for temperature monitoring, potentially enhancing the treatment outcomes.**

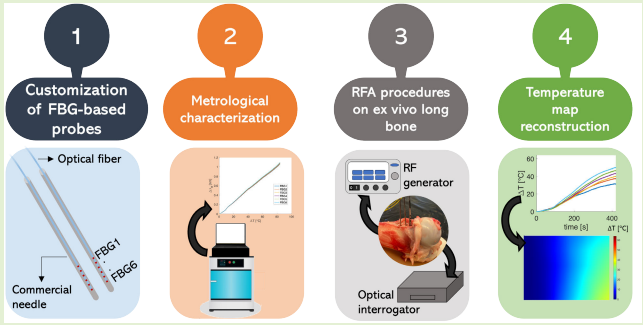

***Index Terms*— Bone cancer, fiber Bragg grating (FBG), radio frequency ablation (RFA), skeletal disease, temperature map, temperature monitoring.**

Manuscript received 21 November 2023; revised 19 December 2023; accepted 23 December 2023. Date of publication 3 January 2024; date of current version 13 February 2024. The associate editor coordinating the review of this article and approving it for publication was Prof. Arnaldo Gomes Leal-Junior. *(Corresponding author: Emiliano Schena.)*

Francesca De Tommasi is with the Unit of Measurements and Biomedical Instrumentation, Departmental Faculty of Engineering, Università Campus Bio-Medico di Roma, 00128 Rome, Italy.

Emiliano Schena is with the Unit of Measurements and Biomedical Instrumentation, Departmental Faculty of Engineering, Università Campus Bio-Medico di Roma, 00128 Rome, Italy, and also with the Unit of Traumatology and Sports Medicine, Fondazione Policlinico Universitario Campus Bio-Medico, 00128 Rome, Italy (e-mail: e.schena@unicampus.it).

Massimiliano Carassiti is with the Unit of Anesthesia, Intensive Care and Pain Management, School of Medicine, Fondazione Policlinico Universitario Campus Bio-Medico, 00128 Rome, Italy.

Paul Jutte is with the Department of Orthopedic Surgery, University Medical Center Groningen, 9713 GZ Groningen, The Netherlands.

Venkatasubramanian Kalpathy Venkiteswaran is with the Surgical Robotics Laboratory, Department of Biomechanical Engineering, University of Twente, 7500 AE Enschede, The Netherlands.

Sarthak Misra is with the Surgical Robotics Laboratory, Department of Biomechanical Engineering, University of Twente, 7500 AE Enschede, The Netherlands, and also with the Surgical Robotics Laboratory, Department of Biomedical Engineering, University of Groningen and University Medical Center Groningen, 9713 GZ Groningen, The Netherlands.

Digital Object Identifier 10.1109/JSEN.2023.3347471

I. Introduction

OSTEOID osteoma (OO) ranks as the third most prevalent benign neoplasm, accounting for the 15% of all the skeletal system malignancies [1], [2]. Males are more commonly affected by OO than women, especially earlier in life (usually between 7 and 25 years old) [3]. OO typically occurs in diaphysis and metaphysis of long bones (i.e., femur and tibia) [4]. Despite their benign nature, OO is extremely painful, especially at night, thus causing insomnia for the affected patient and worsening their quality of life [5]. Until a few years ago, surgery was the leading option for managing OO [6], [7], [8]. However, the reported difficulties in localizing the lesion during surgery often lead to a partial resection, and as a result, pain complaints are occasionally relieved [9]. This shortcoming and the patient's drawn-out recovery have paved the way for the growing popularity of image-guided minimally invasive procedures [10].

Thermal ablation treatments (TATs) based on hyperthermia are good alternatives in the aforementioned scenario [11], [12], [13]. The reduced hospitalization time, the short patient convalescence, and their effectiveness in lowering pain endow these techniques with considerable potential in caring for patients affected by OO [13]. The fundamental goal of TATs

lies in completely destroying malignant cells by turning their temperature to a cytotoxic level (higher than 50 °C) [14]. Currently adopted TATs are radio frequency ablation (RFA), laser interstitial thermotherapy (LITT), microwave ablation (MWA), and high-intensity focused ultrasound (HIFU) [15], [16], [17], [18]. Among them, extensive research suggests RFA as the preferred therapy for OO neoplasms refractory to conventional therapy [9], [19]. During RFA, an active electrode delivers a high-frequency alternating current to the tumor tissue (usually between 350 and 500 kHz). The tissue around the electrode tip is ionically stirred by the applied current, resulting in the tissue heating due to the Joule effect [20].

Since the quantity of damaged volume relies strictly on temperature values reached in the treated tissue and whose persistence over time [21], temperature monitoring during RFA (and generally during TATs) may be paramount. Indeed, temperature feedback allows for ensuring damage to the tumor tissue without harming surrounding healthy tissue, especially for OO located near vital structures like nerves and blood vessels [22]. As a result, gaining temperature data would be beneficial in determining the best treatment parameters and attaining the best match between the malignant and damaged volumes. For these reasons, over the years, a great deal of research has been done finding suitable techniques for temperature monitoring during TATs [23]. Among various alternatives proposed, thermocouples and thermistors are the most widely used during RFA in bone [24], [25], [26], [27], [28], [29], [30].

State-of-the-art solutions range from temperature monitoring using thermocouples directly embedded in the RF probe [29] to the use of thermocouples/thermistors as standalone systems for tracking temperature even far from the applicator [24], [25], [26], [27], [28], [30]. The majority of these investigations monitored temperature primarily for the goal of preserving vulnerable structures close to the malignant tissue, unable to survive cytotoxic temperatures (such as nerve roots) [26], [28], [30], [31], [32]. However, the use of these sensors only enables temperature measurement at a single location, and therefore fails in figuring out the temperature distribution inside the tissue. Because of this, the effectiveness and safety of RFA in bone tumors are still up for debate [33].

In this context, fiber Bragg grating sensors (FBGs) stand out as promising alternatives to fill this gap in the literature to date. The ability of FBGs to be multiplexed within a single optical fiber allows for easily gathering temperature tissue maps with high spatial resolution and good accuracy, outperforming limitations related to the above-mentioned electrical sensors [34]. In TATs, both uniform and chirped FBGs have been employed for monitoring temperature [35], [36]. However, because of the simpler fabrication method and interrogation systems compared to chirped FBGs, uniform ones are generally favored in this application since they offer advantages in terms of cost and complexity. Despite the widespread use of uniform FBGs for monitoring temperature during TATs in several organs (such as liver and kidney) [36], [37], [38], [39], their use in bone tissue is severely restricted [40]. To the best of our knowledge, this is the first investigation using FBGs to evaluate RFA-induced thermal effects in bone.

In this article, we present a pioneering investigation into temperature monitoring using FBGs during RFA in bone tissue. Experiments are carried out on ex vivo porcine femurs, encompassing both the diaphysis and the metaphysis, to emulate RFA in the specific anatomical sites where OO commonly occurs. Six FBGs embedded within two commercial needles are used to estimate tissue temperature at twelve distinct points. The proposed approach contributes significantly to understanding the efficacy of RFA in bone tissue, enabling for the first time the reconstruction of the temperature distribution in a scenario mimicking RFA of OO. By introducing this robust method for temperature monitoring, our work stands out for its remarkable impact, promising to substantially improve treatment outcomes in this application.

II. FBG-Based Probes for Temperature Measurements

A. FBG's Working Principle

An FBG represents a resonant etching imprinted into a small segment of the optical fiber core. When a broadband light signal hits the fiber, this part, referred to as grating, exhibits the ability to reflect specific wavelengths of light, while allowing other wavelengths to pass through. A permanent refractive index modulation along the fiber's propagation axis accomplishes this property. The backreflected narrow spectrum of the incident light is centered at the Bragg wavelength (λ_B), which is a function of the effective refractive index (n_{eff}) and the grating period (Λ) according to the following equation [41]:

$$\lambda_B = 2\, n_{\text{eff}} \Lambda. \tag{1}$$

The fundamental principle of the FBG is based on the λ_B variation, resulting in a shift ($\Delta\lambda_B$) once the grating gets exposed to strain (ϵ) or temperature variations (ΔT). This shift is described by the equation below

$$\Delta\lambda_B = 2\left[\Lambda\frac{\partial n_{\text{eff}}}{\partial \epsilon} + n_{\text{eff}}\frac{\partial \Lambda}{\partial \epsilon}\right]\Delta\epsilon + 2\left[\Lambda\frac{\partial n_{\text{eff}}}{\partial T} + n_{\text{eff}}\frac{\partial \Lambda}{\partial T}\right]\Delta T. \tag{2}$$

In (2), the effects of strain and temperature on the optical fiber are represented by $2[\Lambda(\partial n_{\text{eff}}/\partial\epsilon) + n_{\text{eff}}(\partial\Lambda/\partial\epsilon)]\Delta\epsilon$ and $2[\Lambda(\partial n_{\text{eff}}/\partial T) + n_{\text{eff}}(\partial\Lambda/\partial T)]\Delta T$, respectively. Contributions related to ϵ and ΔT can be split by employing specific configurations (i.e., temperature-free or strain-free) [34]. In the case of TATs, strain-free configurations are adopted to retrieve temperature variations experienced by the tissue during the procedure. In this case, the $\Delta\lambda_B$ shift is obtained by the following equation:

$$\Delta\lambda_B = S_T \Delta T \tag{3}$$

where S_T is the thermal sensitivity, generally equal to 0.010 nm·°C^{-1} [36].

B. Fabrication of the FBG-Based Probes

Two commercial 18 G (ϕ = 1.27 mm) needles manufactured of stainless steel (Laborxing, Shenzhen, China) serve to develop the FBG-based probes (hereinafter Probes 1 and 2). An acrylate-coated optical fiber housing an array of six FBGs is included in each needle. In both arrays, FBGs are 1 mm long and 2 mm apart from edge to edge, giving a total sensitive length coverage of 16 mm and nominally identical in terms of Bragg wavelengths chosen (i.e., 1510 nm, FBG1; 1520 nm, FBG2; 1530 nm, FBG3; 1540 nm, FBG4; 1550 nm, FBG5; 1560 nm, FBG6). The optical fiber positioning inside the needle is such that the sixth FBG is fixed 5 mm from its

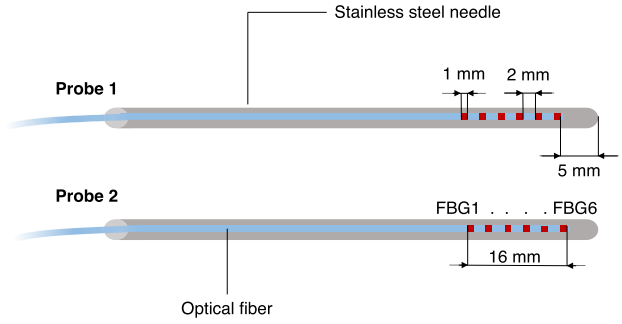

Fig. 1. Customized FBG-based probes embedding six FBGs each served for temperature monitoring during RFA.

tip. Before the encapsulation, the sensitive portion of each fiber is covered by a thermal paste (HY510, Tianhaixing), thus allowing thermal contact between the fiber itself and the metallic needle. Glue is deployed at the extremity near the tip to prevent unintentional movements of the optical fiber inside the needle. The remaining part of the optical fiber sticking out on the proximal needle side is strengthened by means of a flexible tube of 900 μm in diameter up to the optical connector (the system is shown in Fig. 1).

C. Metrological Characterization

1) Static Characterization: Since embedding FBGs inside other material (i.e., stainless steel needles) can affect their thermal response, the FBGs' calibration is carried out to quantitatively assess whether S_T of each FBG is altered after the fabrication process compared to the one provided by the manufacturer (0.010 nm·°C^{-1}). To achieve this, a laboratory oven (PN120 Carbolite) is used to subject the two probes to a controlled temperature variation spanning from 26 °C to 110 °C. Reference temperatures over time are recorded using a k-type thermocouple (Testo SE & Company, KGaA, Lenzkirch, Germany) with a sampling rate of 0.1 Hz, while the output of each probe is acquired through an optical interrogator (si255 Micrometer Optics Inc., USA) set at a constant frequency of 100 Hz.

To calculate the calibration curve ($\Delta\lambda_B$ versus ΔT), the $\Delta\lambda_B$ values of each FBG belonging to each probe are plotted against the corresponding ΔT values (Fig. 2). As a result, the S_T values are calculated from the slope of the fitting lines closely aligning with the experimental data. The goodness of interpolation is evaluated using the correlation coefficient (R^2).

Table I reports the S_T values for each FBG embedding in both probes (Probes 1 and 2). Results suggest an increase in the S_T values for all the FBGs, especially for the ones belonging to Probe 2, after customizing the optical fibers in the needles.

2) Step Response of FBG-Based Probes: As the integration of the FBGs within a metallic needle can impact their response time, the step response of each FBG is experimentally estimated. To apply a temperature step, the two probes are transferred from room temperature (22 °C) to a warm bath at 50 °C. The FBGs' response time (τ) is estimated using the natural logarithm of the error function ($\Gamma(t)$) defined in the following equation:

$$\Gamma(t) = \frac{y(t) - y_\infty}{y(0) - y_\infty} = e^{\frac{-t}{\tau}} \tag{4}$$

where $y(t)$ are the output values of each FBG at a generic t instant, $y(0)$ represents the ones at the beginning of the step,

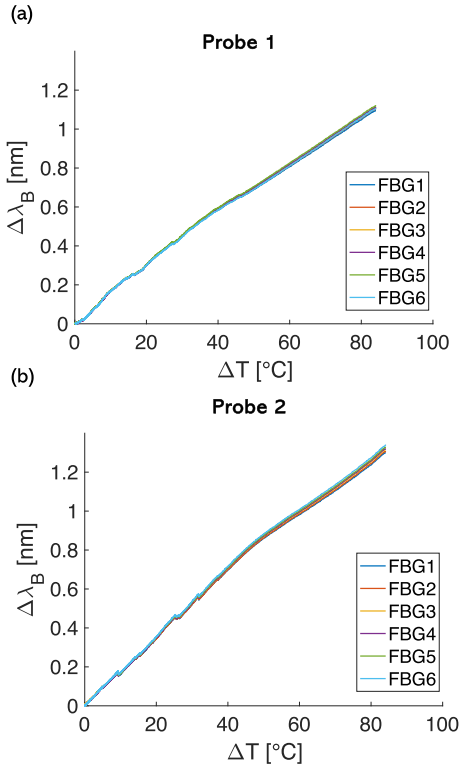

Fig. 2. (a) Bragg wavelength shift ($\Delta\lambda_B$) versus temperature variation (ΔT) trends obtained during the characterization process for each FBG sensor (i.e., FBG1, FBG2, FBG3, FBG4, FBG5, and FBG6) embedded in Probe 1 and (b) Probe 2.

TABLE I
THERMAL SENSITIVITY VALUES (S_T) AND CORRELATION COEFFICIENTS (R^2) FOR EACH OF THE SIX FBG SENSORS (FROM FBG1 TO FBG6) IN PROBES 1 AND 2

	Probe 1		Probe 2	
	S_T [nm ·°C^{-1}]	R^2	S_T [nm ·°C^{-1}]	R^2
FBG1	0.014	0.995	0.016	0.997
FBG2	0.014	0.995	0.016	0.997
FBG3	0.014	0.995	0.017	0.997
FBG4	0.014	0.995	0.017	0.997
FBG5	0.014	0.995	0.017	0.997
FBG6	0.014	0.995	0.017	0.997

and y_∞ the outputs at the steady state. Results show τ ranging between $\sim$ 230 and $\sim$ 560 ms.

III. RFA IN EX VIVO PORCINE BONE

A. Experimental Setup

RFA procedures are performed using the Cool-tip RF ablation system (Covidien, Minneapolis, Minnesota, USA). The RF electrode (single electrode kit E Series, Covidien, Minneapolis, Minnesota, USA), consisting of a 17 G needle internally cooled with a 20-mm active component, can be controlled by the RF generator to provide the required power inside the tissue during the desired time.

Ex vivo porcine femurs, freshly excised, are used to mimic the real ablation procedures. Before starting, bone tissue is drilled to create cavities for housing the RF electrode and FBG-based probes for temperature monitoring. Once the cavity for the RF needle is created, the remaining holes to accommodate the probes are spaced at a distance of 5 and 10 mm along the same axis (see Fig. 3), measured by a digital caliper at each test. This configuration enables capturing

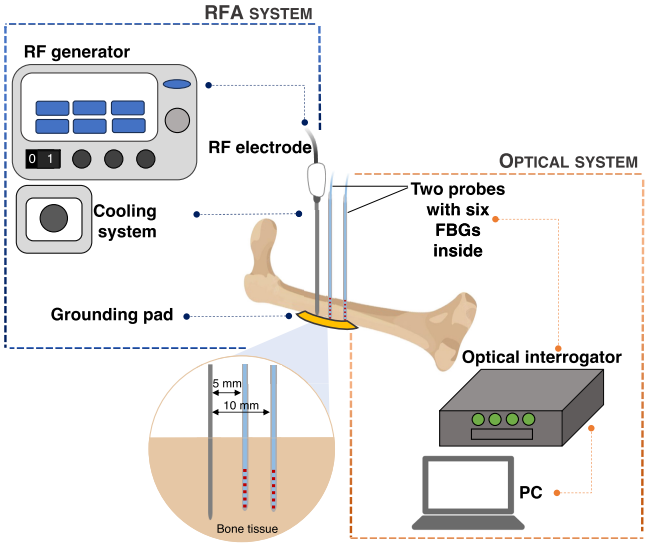

Fig. 3. Schematic representation of the experimental setup employed during ex vivo porcine bone experiments.

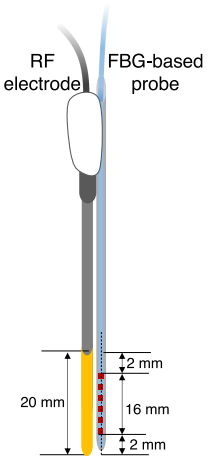

Fig. 4. Relative positioning of the FBG arrays in each probe with respect to the RF electrode active length.

temperature variations even far from the RF electrode, where measurements are usually neglected in current clinical practice. Landmarks on the electrode and FBG-based probes are fixed in such a way that the FBGs cover the central part of the active length, leaving 2 mm on the top and the bottom, since each probe's six FBGs can cover a length of 16 mm (as shown in Fig. 4).

To compare the effects of different energy levels on the thermal response of bone tissue, experiments are executed at two distinct powers (i.e., 25 and 50 W) for the same treatment period (i.e., 7 min −420 s). Both the metaphysis and diaphysis anatomical portions are treated for each of the proposed settings (25 W for 7 min and 50 W for 7 min) for a total of four trials. To complete the electrical circuit, a grounding pad is positioned on the lower bone surface (see Fig. 3).

During the trials, FBGs's output is collected at a sampling frequency of 100 Hz through an optical interrogator (FBG-scan 804D by FBGs International, Geel, Belgium).

B. Data Analysis and Results

1) Temperature Trends: Data recorded by each FBG (from one to six) in Probes 1 and 2 are postprocessed in MATLAB

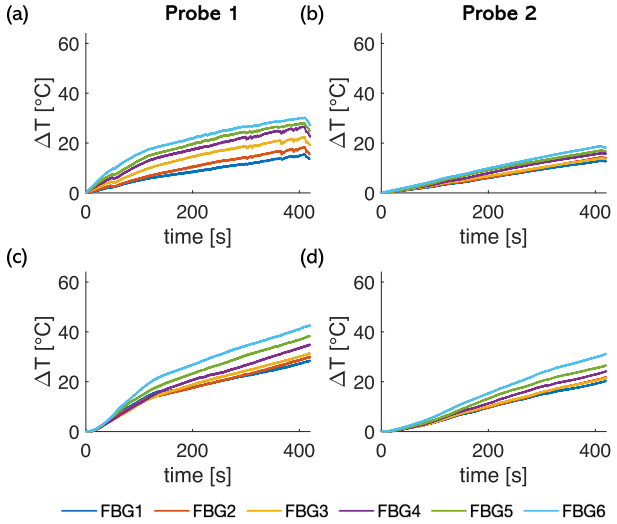

Fig. 5. Temperature variation (ΔT) profiles as a function of time (expressed in s) recorded during the tests performed at 25 W [(a) and (b)] and at 50 W [(c) and (d)] by each FBG embedded in Probe 1 [(a) and (c)] and Probe 2 [(b) and (d)] metaphysis anatomical area.

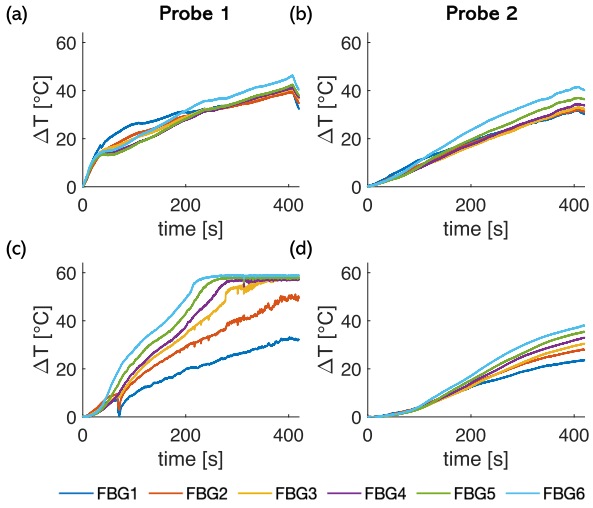

Fig. 6. Temperature variation (ΔT) profiles as a function of time (expressed in s) recorded during the tests performed at 25 W [(a) and (b)] and at 50 W [(c) and (d)] by each FBG embedded in Probe 1 [(a) and (c)] and Probe 2 [(b) and (d)] diaphysis anatomical area.

environment. According to the S_T values obtained during the metrological characterization, ΔT values are retrieved from $\Delta\lambda_B$ gathered by each FBG using (3). Fig. 5 reports the ΔT trends as a function of time recorded during the test performed at 25 W [Fig. 5(a) and (b)] and 50 W [Fig. 5(c) and (d)] for the same treatment time (i.e., 7 min) collected by Probe 1 [Fig. 5(a) and (c)] and Probe 2 [Fig. 5(b) and (d)] in the metaphyseal bone. Instead, Fig. 6 shows the results (ΔT versus time) for 25 W [Fig. 6(a) and (b) and 50 W [Fig. 6(c) and (d)] in the diaphyseal bone. The trend observed by each FBG is marked by a different color in each subplot. For all trials and both probes, it is noticeable that the highest temperature values are recorded by FBG6, the one closest to the tip of the RF applicator. Specifically, the maximum ΔT (i.e., ΔT_{max}) for the test performed at 25 W is 30.1 °C and 46.4 °C for metaphyseal and diaphyseal part, respectively. ΔT_{max} retrieved for trials carried out at 50 W varies between 42.6 °C and 58.9 °C. By comparing ΔT_{max} in trials performed on the same anatomical portion, those operated at 50 W record greater values (42.6 °C versus 30.1 °C for the metaphysis and

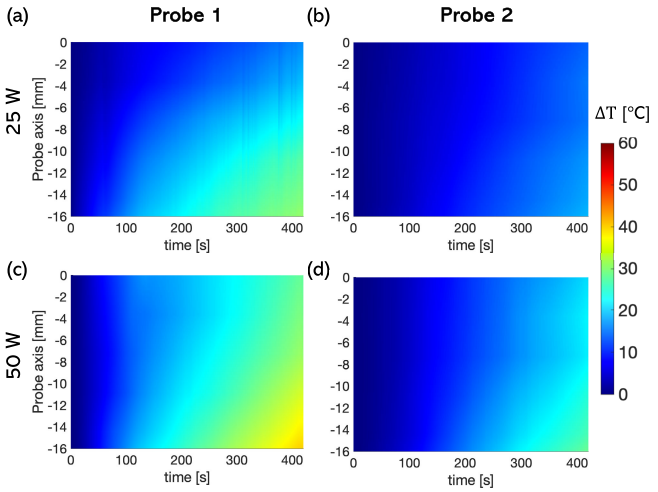

Fig. 7. Temperature variations (ΔT) as a function of time for the tests carried out at 25 W [(a) and (b)] and at 50 W [(c) and (d)] recorded by Probe 1 [(a) and (c)] and Probe 2 [(b) and (d)] metaphysis anatomical area reported as color maps.

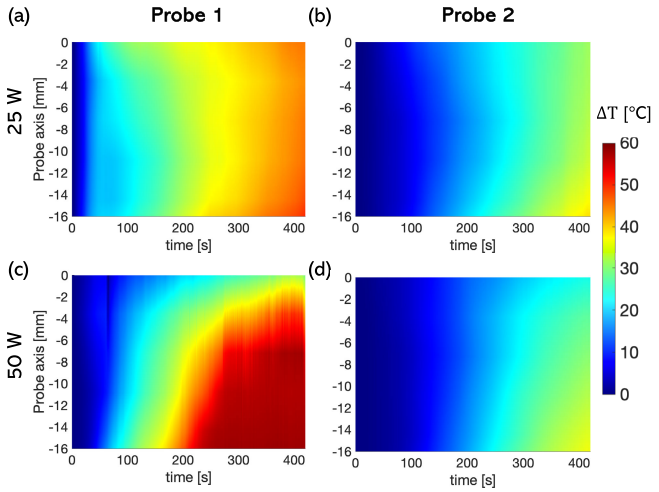

Fig. 8. Temperature variations (ΔT) as a function of time for the tests carried out at 25 W [(a) and (b)] and at 50 W [(c) and (d)] recorded by Probe 1 [(a) and (c)] and Probe 2 [(b) and (d)] diaphysis anatomical area reported as color maps.

58.9 °C versus 46.4 °C), with a difference up to 12.5 °C. Gradually decreasing temperature readings are obtained from FBGs 5, 4, 3, 2, and 1 as they are increasingly far from the RF tip. Except for the ΔT profiles acquired from Probes 1 and 2 in the test carried out at 25 W in the anatomical area of the diaphysis [see Fig. 6(a) and (b)], each investigation confirm this tendency. In general, lower ΔT values are recorded for FBGs belonging to Probe 2 [see Figs. 5(b) and Fig. d) and 6(d)], as this is further away from the energy source (i.e., 10 mm). However, this behavior is not confirmed for the test executed on the diaphyseal part at 25 W, where both probes recorded similar ΔT without any significant differences among FBGs. Furthermore, ΔT slopes for all FBGs involved in the measurements increase during the RF heating until reaching the maximum values for tests shown in Figs. 5(a)–(d) and 6(a) and (b). For the trial performed at 50 W in the diaphysis anatomical area [Fig. 6(c)], FBGs 4, 5, and 6 belonging to Probe 1 record a plateau phase after a short halfway of the ablation process toward the end. Depending on the relative positioning of the FBG to the RF applicator tip, a varying amount of time is required to achieve the plateau (i.e., 300, 270, and 250 s). In the same experiment, FBGs belonging to Probe 2 show a ΔT slope [Fig. 6(d)] different from the one recorded by the same probe in the other trials. Indeed, it is possible to observe a negligible ΔT for the first 41 s of the RF heating and a slow rise until the maximum value is reached.

2) Thermal Maps: Moreover, FBGs embedded in Probes 1 and 2 allow for obtaining the temperature distribution over time. A linear interpolation along the ordinates (i.e., probe axis) among the temperatures measured out of the FBGs is used to derive ΔT values over the 16-mm length of the RF probe covered by the gratings. Figs. 7, and 8 display thermal maps retrieved for Probes 1 and 2 in all four trials carried out. These mappings plot ΔT values as color information against time along the x-axis and the FBGs' relative positioning along the probe axis in the ordinates. By comparing Figs. 7 and 8, it is evident that each test shows a thermal map with different shapes depending on the RF power and the anatomical portion treated. In general, for trials carried out in the diaphyseal area, a wider heat propagation is observed as higher temperatures are detected more quickly by each FBG, especially the one belonging to Probe 1.

IV. Discussion and Conclusion

This study addresses a critical gap in the state-of-the-art by investigating temperature assessment during RFA in ex vivo long bone using FBGs. Previous studies lacked comprehensive information on temperature distribution, relying on single-point tracking with thermistors or thermocouples [26], [28], [30], [31], [32], thus failing to determine the thermal gradients occurring in the treated area [42]. In contrast, our approach employs FBGs with multiplexing capabilities, allowing for a more thorough evaluation [34]. Customized stainless-steel needles holding six FBGs each allow for monitoring temperature at twelve locations within the bone and provide insights into thermal gradients established along the RF probe axis. Before the experiments, the metrological properties of the developed probes are assessed by investigating FBG's thermal response. Results reveal S_T values between 0.014 and 0.017 nm·°C^{-1}, higher than those of bare nonencapsulated FBGs [22], [40].

Experiments are carried out on ex vivo porcine femurs since, together with the tibia, it is one of the anatomical regions most severely affected by OO to date [2]. Both the diaphyseal and metaphyseal parts are treated, considering the potential occurrence of the tumor in either region [4]. This is accomplished to assess the impact of different tissue portions on the treatment outcome. RFA procedures are performed at two distinct powers (25 W and 50 W, often adopted in clinical scenarios [43], [44]) for a treatment duration of 7 min. Each setting is applied to both diaphysis and metaphysis, resulting in a total of four trials. Temperature monitoring using Probes 1 and 2 positioned at 5 and 10 mm from the RF applicator provide temperature data over a large tissue area. ΔT profiles over time (Figs. 5 and 6) show higher ΔT in trials at 50 W compared to those at 25 W. FBG6 (i.e., the one close to the RF applicator tip) consistently record ΔT_{max} in all trials. Moreover, it is possible to observe nonuniform temperature trends along the sensitive portion of each probe, thus highlighting an uneven heat diffusion along the active portion of the RF applicator. Substantial differences can be observed among the ΔT_{max} values recorded by each FBG from the same probe at the end of the procedure, evidencing high thermal gradients established in a small portion of tissue

(up to 28 °C). These findings underscore the inadequacy of electric sensors in this application, given their ability to provide data at a single point, consequently overlooking temperature dynamics along the tissue portion covered by the RF probe. Then, temporal temperature distributions are also reconstructed for each test and FBG-based probe employed by means of a linear interpolation between ΔT values recorded by each sensor, allowing for heat diffusion visualization along the probe axis as a function of time (see Figs. 7 and 8). The significance of this reconstruction lies in its potential to estimate the inflicted thermal damage, as this is dependent on the temperature values measured and the exposure period [21]. Results reveal a change in the temperature distribution shape according to the power input and the anatomical area treated. In general, in trials performed in the metaphyseal area, heat propagation is found to be wider for both the 25- and 50-W tests than those performed on the diaphyseal part for the same settings. This is evident since both Probes 1 and 2 record higher ΔT for extended durations.

In conclusion, the implementation of FBGs for temperature monitoring during bone RFA tackled a significant gap in the literature. The temporal distribution of temperature within the bone can be thoroughly examined during the experiments, thanks to the multiplexing abilities of FBGs, resulting in important insights into the effects of RFA in long bones. Our evidence has the potential to improve RFA outcomes for bone cancer. By implementing temperature monitoring systems during RFA such as the ones proposed in this paper, ablation settings may be fine-tuned toward achieving optimum tumor destruction and minimizing damage to surrounding anatomical structures. This work advances existing research efforts aimed at improving ablation therapy for bone tumor resection. However, further stages are still required to fully grasp how several parameters may affect the clinical outcome in this challenging application.

REFERENCES

[1] K. I. Atesok, B. A. Alman, E. H. Schemitsch, A. Peyser, and H. Mankin, "Osteoid osteoma and osteoblastoma," *J. Amer. Acad. Orthopaedic Surgeons*, vol. 19, no. 11, pp. 678–689, 2011.

[2] S. Noordin et al., "Osteoid osteoma: Contemporary management," *Orthopedic Rev.*, vol. 10, no. 3, p. 7496, Sep. 2018.

[3] W. G. Ward, J. J. Eckardt, S. Shayestehfar, J. Mirra, T. Grogan, and W. Oppenheim, "Osteoid osteoma diagnosis and management with low morbidity," *Clin. Orthopaedics Rel. Res.*, vol. 291, pp. 229–235, Jun. 1993.

[4] A. Greenspan, "Benign bone-forming lesions: Osteoma, osteoid osteoma, and osteoblastoma: Clinical, imaging, pathologic, and differential considerations," *Skeletal Radiol.*, vol. 22, no. 7, pp. 485–500, Oct. 1993.

[5] N. Laurence, M. Epelman, R. I. Markowitz, C. Jaimes, D. Jaramillo, and N. A. Chauvin, "Osteoid osteomas: A pain in the night diagnosis," *Pediatric Radiol.*, vol. 42, no. 12, pp. 1490–1501, Dec. 2012.

[6] F. Franceschi, A. Marinozzi, R. Papalia, U. G. Longo, G. Gualdi, and E. Denaro, "Intra- and juxta-articular osteoid osteoma: A diagnostic challenge: Misdiagnosis and successful treatment: A report of four cases," *Arch. Orthopaedic Trauma Surgery*, vol. 126, no. 10, pp. 660–667, Oct. 2006.

[7] G. Rizzello, U. G. Longo, N. Maffulli, and V. Denaro, "Arthroscopic removal of an intraarticular osteoid osteoma of the distal tibia," *J. Foot Ankle Surgery*, vol. 49, no. 4, p. 398, Jul. 2010.

[8] A. Giombini, S. Dragoni, T. Averna, M. Ripani, U. Longo, and N. Maffulli, "Osteoid osteoma mimicking overuse syndromes in athletes," *J. Sports Med. Phys. Fitness, The*, vol. 49, no. 2, p. 167, Jun. 2009.

[9] C. P. Cantwell, J. Obyrne, and S. Eustace, "Current trends in treatment of osteoid osteoma with an emphasis on radiofrequency ablation," *Eur. Radiol.*, vol. 14, no. 4, pp. 607–617, Apr. 2004.

[10] A. Tomasian, R. L. Cazzato, K. Sharma, A. Gangi, and J. W. Jennings, "Benign bone tumors: State of the art in minimally invasive percutaneous interventions," *RadioGraphics*, vol. 43, no. 2, Feb. 2023, Art. no. e220041.

[11] D. Rosenthal and M. R. Callstrom, "Critical review and state of the art in interventional oncology: Benign and metastatic disease involving bone," *Radiology*, vol. 262, no. 3, pp. 765–780, Mar. 2012.

[12] A. Tomasian and J. W. Jennings, "Bone metastases: State of the art in minimally invasive interventional oncology," *RadioGraphics*, vol. 41, no. 5, pp. 1475–1492, Sep. 2021.

[13] D. Motamedi et al., "Thermal ablation of osteoid osteoma: Overview and step-by-step guide," *RadioGraphics*, vol. 29, no. 7, pp. 2127–2141, Nov. 2009.

[14] K. F. Chu and D. E. Dupuy, "Thermal ablation of tumours: Biological mechanisms and advances in therapy," *Nature Rev. Cancer*, vol. 14, no. 3, pp. 199–208, Mar. 2014.

[15] D. P. Barei, G. Moreau, M. T. Scarborough, and M. D. Neel, "Percutaneous radiofrequency ablation of osteoid osteoma," *Clin. Orthopaedics Rel. Res.*, vol. 373, pp. 115–124, Apr. 2000.

[16] A. Gangi, H. Alizadeh, L. Wong, X. Buy, J.-L. Dietemann, and C. Roy, "Osteoid osteoma: Percutaneous laser ablation and follow-up in 114 patients," *Radiology*, vol. 242, no. 1, pp. 293–301, Jan. 2007.

[17] K. V. Sharma et al., "Comparison of noninvasive high-intensity focused ultrasound with radiofrequency ablation of osteoid osteoma," *J. Pediatrics*, vol. 190, pp. 222–228, Nov. 2017.

[18] E. S. Rinzler, G. M. Shivaram, D. W. Shaw, E. J. Monroe, and K. S. H. Koo, "Microwave ablation of osteoid osteoma: Initial experience and efficacy," *Pediatric Radiol.*, vol. 49, no. 4, pp. 566–570, Apr. 2019.

[19] R.-T. Hoffmann et al., "Radiofrequency ablation in the treatment of osteoid osteoma-5-year experience," *Eur. J. Radiol.*, vol. 73, no. 2, pp. 374–379, 2010.

[20] S. N. Goldberg, G. S. Gazelle, and P. R. Mueller, "Thermal ablation therapy for focal malignancy: A unified approach to underlying principles, techniques, and diagnostic imaging guidance," *Amer. J. Roentgenol.*, vol. 174, no. 2, pp. 323–331, 2000.

[21] J. A. Pearce, "Comparative analysis of mathematical models of cell death and thermal damage processes," *Int. J. Hyperthermia*, vol. 29, no. 4, pp. 262–280, Jun. 2013.

[22] F. De Tommasi, C. Massaroni, R. F. Grasso, M. Carassiti, and E. Schena, "Temperature monitoring in hyperthermia treatments of bone tumors: State-of-the-art and future challenges," *Sensors*, vol. 21, no. 16, p. 5470, Aug. 2021.

[23] P. Saccomandi, E. Schena, and S. Silvestri, "Techniques for temperature monitoring during laser-induced thermotherapy: An overview," *Int. J. Hyperthermia*, vol. 29, no. 7, pp. 609–619, Nov. 2013.

[24] F. Rachbauer, J. Mangat, G. Bodner, P. Eichberger, and M. Krismer, "Heat distribution and heat transport in bone during radiofrequency catheter ablation," *Arch. Orthopaedic Trauma Surgery*, vol. 123, nos. 2–3, pp. 86–90, Apr. 2003.

[25] R. G. Bitsch, R. Rupp, L. Bernd, and K. Ludwig, "Osteoid osteoma in an ex vivo animal model: Temperature changes in surrounding soft tissue during CT-guided radiofrequency ablation," *Radiology*, vol. 238, no. 1, pp. 107–112, Jan. 2006.

[26] A. Adachi et al., "Heat distribution in the spinal canal during radiofrequency ablation for vertebral lesions: Study in swine," *Radiology*, vol. 247, no. 2, pp. 374–380, May 2008.

[27] H. Nijland, J. Zhu, T. Kwee, D. Hao, and P. Jutte, "Experiments on physical ablation of long bone using microwave ablation; defining optimal settings using ex- and in-vivo experiments," *PLoS ONE*, vol. 18, no. 4, Apr. 2023, Art. no. e0284027.

[28] P. S. Pezeshki et al., "Evaluation of a bipolar-cooled radiofrequency device for ablation of bone metastases: Preclinical assessment in porcine vertebrae," *Spine J.*, vol. 14, no. 2, pp. 361–370, Feb. 2014.

[29] A. Greenberg, T. Berenstein Weyel, J. Sosna, J. Applbaum, and A. Peyser, "The distribution of heat in bone during radiofrequency ablation of an ex vivo bovine model of osteoid osteoma," *Bone Joint J.*, vol. 96, no. 5, pp. 677–683, May 2014.

[30] W. Zhao et al., "Thermal effect of percutaneous radiofrequency ablation with a clustered electrode for vertebral tumors: In vitro and vivo experiments and clinical application," *J. Bone Oncol.*, vol. 12, pp. 69–77, Sep. 2018.

[31] R. Lecigne et al., "Transforaminal insertion of a thermocouple on the posterior vertebral wall combined with hydrodissection during lumbar spinal radiofrequency ablation," *Amer. J. Neuroradiol.*, vol. 40, no. 10, pp. 1786–1790, Sep. 2019.
[32] A. Nakatsuka et al., "Percutaneous radiofrequency ablation of painful spinal tumors adjacent to the spinal cord with real-time monitoring of spinal canal temperature: A prospective study," *CardioVascular Interventional Radiol.*, vol. 32, no. 1, pp. 70–75, Jan. 2009.
[33] E. Lanza et al., "Osteoid osteoma treated by percutaneous thermal ablation: When do we fail? A systematic review and guidelines for future reporting," *CardioVascular Interventional Radiol.*, vol. 37, no. 6, pp. 1530–1539, Dec. 2014.
[34] D. Lo Presti et al., "Fiber Bragg gratings for medical applications and future challenges: A review," *IEEE Access*, vol. 8, pp. 156863–156888, 2020.
[35] S. Korganbayev et al., "Thermal profile detection through high-sensitivity fiber optic chirped Bragg grating on microstructured PMMA fiber," *J. Lightw. Technol.*, vol. 36, no. 20, pp. 4723–4729, Oct. 2018.
[36] E. Schena, D. Tosi, P. Saccomandi, E. Lewis, and T. Kim, "Fiber optic sensors for temperature monitoring during thermal treatments: An overview," *Sensors*, vol. 16, no. 7, p. 1144, Jul. 2016.
[37] D. Tosi et al., "Monitoring of radiofrequency thermal ablation in liver tissue through fibre Bragg grating sensors array," *Electron. Lett.*, vol. 50, no. 14, pp. 981–983, Jul. 2014.
[38] E. De Vita et al., "Investigation of the heat sink effect during microwave ablation in hepatic tissue: Experimental and numerical analysis," *IEEE Sensors J.*, vol. 21, no. 20, pp. 22743–22751, Oct. 2021.
[39] G. Palumbo et al., "Temperature profile of ex-vivo organs during radio frequency thermal ablation by fiber Bragg gratings," *J. Biomed. Opt.*, vol. 21, no. 11, Nov. 2016, Art. no. 117003.
[40] E. De Vita et al., "Multipoint temperature monitoring of microwave thermal ablation in bones through fiber Bragg grating sensor arrays," *Sensors*, vol. 20, no. 11, p. 3200, Jun. 2020.
[41] T. Erdogan, "Fiber grating spectra," *J. Lightw. Technol.*, vol. 15, no. 8, pp. 1277–1294, Aug. 1997.
[42] F. De Tommasi et al., "Fiber Bragg gratings for temperature measurements under thermal gradients: Comparison between two different lengths," *IEEE Trans. Instrum. Meas.*, vol. 72, pp. 1–10, 2023.
[43] N. Toyota et al., "Radiofrequency ablation therapy combined with cementoplasty for painful bone metastases: Initial experience," *CardioVascular Interventional Radiol.*, vol. 28, no. 5, pp. 578–583, Jun. 2005.
[44] S. Masala et al., "Radiofrequency heat ablation and Vertebroplasty in the treatment of neoplastic vertebral body fractures," *Anticancer Res.*, vol. 24, no. 5B, pp. 3129–3134, 2004.

Francesca De Tommasi (Student Member, IEEE) received the M.Sc. (cum laude) degree in biomedical engineering from the Università Campus Bio-Medico di Roma (UCBM), Rome, Italy, in 2020, where she is currently pursuing the Ph.D. degree in bioengineering with the Unit of Measurements and Biomedical Instrumentation, Rome.

Her research interests focus on the development of FBG-based measurement systems for patient safety enhancement and physiological monitoring.

Emiliano Schena (Senior Member, IEEE) received the master's (cum laude) and Ph.D. degrees in biomedical engineering from the Università Campus Bio-Medico di Roma (UCBM), Rome, Italy, in 2006 and 2009, respectively.

He is currently a Full Professor with the Department of Engineering, UCBM. He has directed a number of national and international research projects. His main research interests include systems for monitoring physiological parameters, the application of fiber-optic sensors in medicine, and laser ablation for cancer removal.

Massimiliano Carassiti received the master's (Hons.) degree in medicine and surgery from the University of Rome, Rome, Italy, in 1987, and the Ph.D. degree from the Clinical University of Navarra, Pamplona, Spain.

He is currently an Anesthesiologist with the Unit of Anesthesia, Intensive Care and Pain Management, Fondazione Policlinico Universitario Campus Bio-Medico, Rome, Italy, and an Associate Professor of Anesthesia at the Università Campus Bio-Medico di Roma (UCBM), Rome. He is also one of the Co-Founder of the HEREMOS spin-off. His main clinical and research interests include anesthesiology, intensive care medicine, and pain medicine and management.

Paul Jutte received the M.D. and Ph.D. degrees. His Ph.D. was on spinal tuberculosis from 2000 to 2006.

He has been an Orthopedic Surgeon since 2003. He completed the Fellowship in Orthopedic Oncology in Bologna Italy, in 2003, and Los Angeles, CA, USA, in 2005. He is currently a Full Professor in Orthopedic Surgery and the Department Head of the University Medical Center Groningen, Groningen, The Netherlands. He founded a regional clinical network for orthopedic infections and osteoarthritis care and holds several chair positions. He has published over 200 peer-reviewed articles (H-factor > 40) and is the Co-Program Leader of Man Biomaterials Microbes (MBM), a research line at the W. J. Kolff Institute, University of Groningen, Groningen. His current clinical research work is aimed at minimizing tissue damage, improving diagnosis, and the safety and efficacy of surgical treatment of tumors and infections.

Venkatasubramanian Kalpathy Venkiteswaran (Member, IEEE) received the Ph.D. degree in mechanical engineering from The Ohio State University, Columbus, OH, USA, in 2017.

He is currently an Assistant Professor with the Department of Biomechanical Engineering, University of Twente, Enschede, The Netherlands. Before that, he was a Postdoctoral Fellow with the Surgical Robotics Laboratory, University of Twente, for two years. His research interests include the design of soft robots and flexible devices with a focus on medical applications.

Sarthak Misra (Senior Member, IEEE) received the master's degree in mechanical engineering from McGill University, Montreal, QC, Canada, in 2001, and the Ph.D. degree in mechanical engineering from Johns Hopkins University, Baltimore, MD, USA, in 2009.

He is currently a Full Professor with the Department of Biomechanical Engineering, University of Twente, Enschede, The Netherlands, and the Department of Biomedical Engineering, University of Groningen and University, Groningen, The Netherlands, Medical Center Groningen, Groningen. Before commencing the Ph.D. studies, he was a Dynamics and Controls Analyst with the International Space Station Program. His research interests include surgical robotics and medical microrobotics.

Dr. Misra was a recipient of the European Research Council Starting, Proof-of-Concept, and Consolidator Grants and the Netherlands Organization for Scientific Research VENI and VIDI Awards. He was the Co-Chair of the Robotics and Automation Society Technical Committee on Surgical Robotics and the International Federation of Automatic Control Technical Committee on Biological and Medical Systems.